Optical conductivity, Fermi surface, and spin-orbit coupling effects in Sr_2RhO_4

Guoren Zhang[1] and Eva Pavarini[2,3,4]

[1]*Key Laboratory of Materials Physics, Institute of Solid State Physics, Chinese Academy of Sciences,
Hefei 230031, People's Republic of China*
[2]*Institute for Advanced Simulation, Forschungszentrum Jülich, 52425 Jülich, Germany*
[3]*JARA High-Performance Computing, RWTH Aachen University, 52062 Aachen, Germany*
[4]*JARA FIT, RWTH Aachen University, 52062 Aachen, Germany*

By using the local-density approximation + dynamical mean-field theory approach, we study the low-energy electronic properties of Sr_2RhO_4 in a realistic setting, and compare to Sr_2RuO_4. We investigate the interplay of spin-orbit coupling, crystal field, and Coulomb interaction, including the tetragonal terms of the Coulomb tensor. We find that (i) differently than in Sr_2RuO_4, the zero-frequency effective crystal-field "enhancement" due to Coulomb repulsion, $\Delta\varepsilon_{CF}(\omega = 0)$, is small and, depending on the parameters, even *negative*. (ii) In addition, the effects of (realistic) anisotropic Coulomb terms are weak. (iii) Instead, the effective zero-frequency enhancement of the spin-orbit interaction doubles the value of the corresponding local-density approximation couplings. This explains the experimental Fermi surface and supports a previous proposal based on static mean-field calculations. We find that the sign of the Coulomb-induced spin-orbit anisotropy is influenced by the octahedral rotation. Based on these conclusions, we examine recent optical conductivity experiments. (iv) We show that the spin-orbit interaction is key for understanding them; differently than in Sr_2RuO_4, the t_{2g} intraorbital contributions are small; thus, the single-band picture does not apply.

I. INTRODUCTION

Sr_2RhO_4 is a remarkable example of strongly correlated metal. It is a layered perovskite with a crystal structure very similar to that of the unconventional superconductor Sr_2RuO_4 [1], with which it also shares a similar electronic structure—having, however, five instead of four electrons in the t_{2g} shell. Quantum oscillation and angle-resolved photoemission experiments [2,3] yield relatively large mass enhancements, with $m^*/m_e \sim 3$, placing the single-layer rhodate in the family of strongly correlated compounds. Sr_2RhO_4 was a puzzle right after it was synthetized because the experimental Fermi surface substantially disagreed with local-density approximation (LDA) predictions, a very surprising result even for a strongly correlated material.

The riddle was partially solved, taking into account the effects of the rotation of corner-sharing octahedra [4,5]; the structure of Sr_2RhO_4 is shown in Fig. 1. Still, even after the actual crystal structure was used in the calculations, surprisingly, a strong disagreement remained. It was then shown that including the spin-orbit (SO) interaction brings the LDA Fermi surface much closer to experimental data [6]. For the last discrepancies, a possible explanation emerged via LDA+U calculations. It was shown [7] that the Coulomb interaction yields an effective Hartree-Fock enhancement of the SO coupling; indeed, with optimal choices of $U - J$, the experimental and LDA+U Fermi surface can be brought to perfect agreement. Good agreement with experiments was later also obtained in LDA+DMFT (local-density approximation plus dynamical mean-field theory) calculations [8–10], using a hybridization-expansion continuous-time quantum Monte Carlo solver. In one of these works [8], it was suggested that

the LDA+U SO enhancement could be an artefact of the static mean-field approximation. The question remains unresolved, however, since, due to the difficulties of the problem, DMFT calculations had been performed with approximation either in the t_{2g} Hubbard Hamiltonian and/or the Green's function matrix.

Furthermore, recently it was pointed out that approximated versions of the Coulomb tensor, as the one used, e.g., in the above-discussed LDA+U work, can lead to a strong overestimate the Hartree-Fock enhancement of the SO coupling [11]. Finally, nonspherical Coulomb terms were found playing a key role for Sr_2RuO_4 [11], in particular in determining the size of the effective zero-frequency crystal-field splitting, and thus the shape of the Fermi surface, opening the question whether or not they are also important for the single-layered rhodate.

To further complicate the scenario, recent experiments [12] suggest that SO effects are responsible for a midinfrared peak observed in the in-plane conductivity $\sigma_{ab}(\omega)$. Such a peak, identified by the name β by the authors, would then correspond to an inter-band transition rather than being the result of strong-correlation effects, as often assumed in analogous materials. This led the authors, by analogy, to extend the conclusion to layered ruthenates, systems which also exhibit a midinfrared peak similar to β, thus challenging the so-called resilient quasiparticle picture [13]. Such a scenario, however, seems at odds with recent LDA+DMFT results for Sr_2RuO_4 [14]. In the latter, SO effects were found to be stronger at low, rather than intermediate frequency. Furthermore, intraorbital processes were shown to give a large contribution to the optical conductivity, even in the presence of SO interaction.
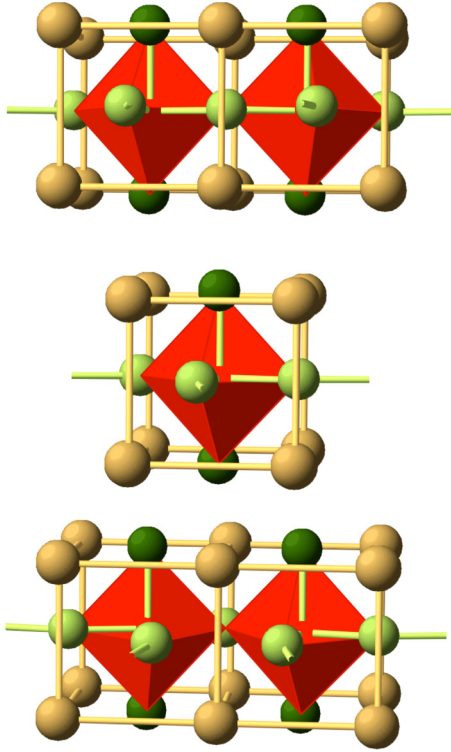
FIG. 1. The $I4_1/acd$ layered tetragonal crystal structure of Sr_2RhO_4. The figure shows perovskite cells in three subsequent layers along the **c** axis and displays the rotation of corner-sharing RhO_6 octahedra [1]. This rotation is absent in Sr_2RuO_4.
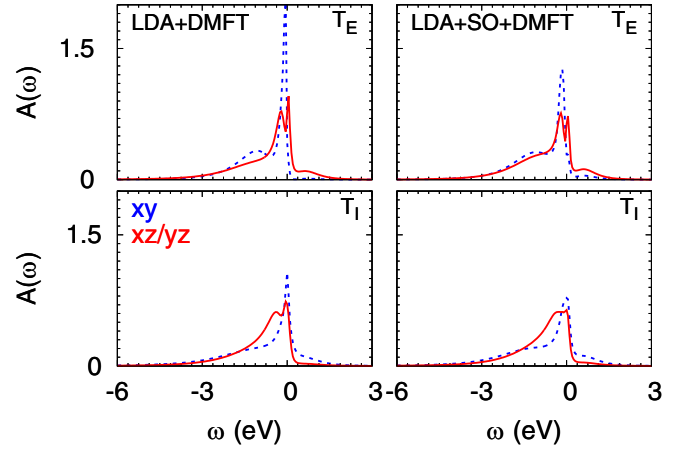

FIG. 2. The diagonal elements of the t_{2g} spectral function matrix for Sr_2RhO_4 in states/eV/formula-unit. Calculations are for $T \sim$ 290 K and $(U, J) = (2.3, 0.4)$ eV for both the idealized tetragonal (T_I) and the experimental tetragonal (T_E) structure. For the latter, the xy states are almost full.

The complex panorama described above calls for revisiting the problem. In this paper, we do this via the LDA+DMFT approach, using a general state-of-the art weak-coupling continuous-time quantum Monte Carlo impurity solver which allows us to deal with general Coulomb vertices and the SO interaction without approximations, neither in the one-electron part of the Hamiltonian nor in the Coulomb tensor.

The paper is organized as follows. In Sec. II we explain model and method. In Sec. III we present the results. We show that the many-body crystal-field "enhancement" plays a small role at the Fermi surface, differently than in the case of for Sr_2RuO_4; furthermore, in some case it is even negative. We show that, in line with LDA+U results, the SO coupling and its enhancement are key. We emphasize that, however, for the same Coulomb parameters, LDA+U calculations overestimate the effect. To single out the effects of octahedral rotations, we present results for both the experimental structure of Sr_2RhO_4 and an idealized structure with no rotation of octahedra, i.e., the crystal structure of Sr_2RuO_4. The associated orbital-resolved spectral functions are shown in Fig. 2. We show that the interplay of distortions and SO interaction is key not only at the Fermi surface, but also for understanding conductivity experiments. We show that intraorbital processes are small for Sr_2RhO_4, differently than for Sr_2RuO_4. This explains the apparent discrepancy between theory and experiments. We show that, however, the SO interaction enhances rather than generates the β peak. Finally, we discuss mass enhancements and scattering rates. The conclusions can be found in Sec. IV. In the Appendix,

we give the Coulomb interaction tensor in the total angular momentum basis, including the terms which do not have the density-density form, often neglected.

II. MODEL AND METHOD

We use the LDA+DMFT approach [15]. First we calculate the electronic structure in the LDA via the full-potential linearized augmented plane-wave method as implemented in WIEN2K code [16]. Then, via the maximally localized Wannier function method [17,18] and t_{2g} projectors, we construct localized t_{2g}-like Wannier functions centered at Rh atoms spanning the t_{2g} bands. Using these Wannier orbitals, we build the t_{2g} Hubbard Hamiltonian,

$$H = -\sum_{ii'\sigma\sigma'} \sum_{mm'} t_{m\sigma,m'\sigma'}^{ii'} \, c_{im\sigma}^{\dagger} c_{i'm'\sigma'}$$

$$+ \frac{1}{2} \sum_{i\sigma\sigma'} \sum_{mm'pp'} U_{mm'pp'} c_{im\sigma}^{\dagger} c_{im'\sigma'}^{\dagger} c_{ip'\sigma'} c_{ip\sigma} - H_{dc}, \quad (1)$$

where $c_{im\sigma}(c_{im\sigma}^{\dagger})$ annihilates (creates) an electron at lattice site i with spin $\sigma \in \{\uparrow, \downarrow\}$ and orbital quantum number $m \in \{xy, yz, xz\}$. The one-electron terms $-t_{mm'}^{ii'}$ yield hopping integrals ($i \neq i'$) and the crystal-field matrix ($i = i'$). We calculate the noninteracting Hamiltonian both without (LDA) and with (LDA+SO) SO interaction. For what concerns the second case, the on-site part of the SO term takes the form

$$H_{SO} = \sum_{i\mu} \sum_{m\sigma m'\sigma'} \lambda_{\mu} \varepsilon_{m\sigma m'\sigma'}^{i\mu} c_{im\sigma}^{\dagger} c_{im'\sigma'},$$

where $\mu = x, y, z$, and

$$\varepsilon_{m\sigma m'\sigma'}^{i\mu} = \langle m\sigma | s_{\mu}^i l_{\mu}^i | m'\sigma' \rangle.$$

We extract the SO couplings by comparing the LDA and LDA+SO Hamiltonians. By ordering the basis as $|xy\rangle_{\uparrow}, |yz\rangle_{\uparrow}, |xz\rangle_{\uparrow}, |xy\rangle_{\downarrow}, |yz\rangle_{\downarrow}, |xz\rangle_{\downarrow}$, the on-site crystal-field

matrix can be then expressed as

$$
\varepsilon = \begin{pmatrix}
\varepsilon_{xy} & 0 & 0 & 0 & \frac{\lambda_y}{2} & -\frac{i\lambda_x}{2} \\
0 & \varepsilon_{yz} & \frac{i\lambda_z}{2} & -\frac{\lambda_y}{2} & 0 & 0 \\
0 & -\frac{i\lambda_z}{2} & \varepsilon_{xz} & \frac{i\lambda_x}{2} & 0 & 0 \\
0 & -\frac{\lambda_y}{2} & -\frac{i\lambda_x}{2} & \varepsilon_{xy} & 0 & 0 \\
\frac{\lambda_y}{2} & 0 & 0 & 0 & \varepsilon_{yz} & -\frac{i\lambda_z}{2} \\
\frac{i\lambda_x}{2} & 0 & 0 & 0 & \frac{i\lambda_z}{2} & \varepsilon_{xz}
\end{pmatrix}.
$$

The diagonal terms are ε_{xz}, ε_{yz}, and ε_{xy}, where $\varepsilon_{xy} = (\varepsilon_{xz} + \varepsilon_{yz})/2 - \varepsilon_{CF}$, and where ε_{CF} is the crystal-field splitting in the absence of SO interaction; the couplings λ_x and λ_y are the SO matrix elements between xy and xz/yz orbitals and λ_z between yz and xz orbitals. We consider two structures. The first is the idealized $I4/mmm$ structure, in which Rh sites have D_{4h} symmetry, and the second is the actual experimental structure, space group $I4_1/acd$ [1]. In the latter, the RhO$_4$ octahedra rotate and Rh sites have symmetry S$_4$. The SO couplings are similar in the two structures; the specific values for the $I4_1/acd$ structure are $\lambda_x = \lambda_y = \lambda_{xy} = 106$ meV and $\lambda_z = 102$ meV. In the idealized structure the crystal-field splitting is very small, it varies from 0 to 50 meV, depending on the specific choice of Wannier functions [19]. In the experimental structure, it is about 108 meV, similar as in Sr$_2$RuO$_4$.

The terms $U_{mm'p'p}$ are elements of the screened Coulomb interaction tensor. In the O(3)-symmetric case, these elements can be expressed as a function of the Slater integrals F_0, F_2, and F_4. For t_{2g} states, the essential terms [15] are the direct [$U_{mm'mm'} = U_{m,m'} = U - 2J(1 - \delta_{m,m'})$] and the exchange ($U_{mm'm'm} = J$) screened Coulomb interaction, the pair-hopping ($U_{mmm'm'} = J$), and the spin-flip term ($U_{mm'm'm} = J$). In these expressions, we used the relations $U = F_0 + \frac{4}{49}(F_2 + F_4)$ and $J = \frac{1}{49}(3F_2 + \frac{20}{9}F_4)$, as appropriate for t_{2g} states [15]. Our calculations are performed in the t_{2g} basis. For comparison, the spherical Coulomb tensor in the total angular momentum basis is given in the Appendix. For tetragonal site symmetry, there are additional parameters. In this paper, we will discuss, in particular, the effect of $\Delta U = U_{xy,xy} - U_{xz,xz}$, which was found to play a key role for Sr$_2$RuO$_4$ [11]. For the the double-counting correction, H_{dc}, we use the around mean-field approximation, as we have established in Refs. [11,14].

We solve the Hamiltonian Eq. (1) with DMFT using continuous-time quantum Monte Carlo [20–23], via the general implementation of the interaction expansion (CT-INT) solver presented in Ref. [23] and extended to explicitly include the SO interaction in Ref. [11]. For Sr$_2$RhO$_4$, cRPA estimates yield $U \sim 2$ eV and $J \sim 0.2 - 0.3$ eV [9,10]. Here we perform calculations for cRPA values and slightly larger ones; we do this to account for the fact that cRPA often overestimates screening effects. Indeed, we do find that slightly larger U and J values yield a better agreement with experimentally available data.

III. RESULTS

A. Spectral function matrix and Fermi surface

The LDA+DMFT and LDA+SO+DMFT spectral function matrix is shown in Fig. 2, both for the idealized (in short, T_I) and the experimental (in short, T_E) tetragonal structure. An important difference between the two structures can be found in the orbital occupations, n_m^σ. In the T_I case, LDA yields $n_{xy}^\sigma \sim 0.74 < n_{xz/yz}^\sigma$, while in the T_E case we obtain $n_{xy}^\sigma \sim 0.96 > n_{xz/yz}^\sigma$. This means that the LDA orbital polarization, $p = \sum_\sigma (n_{xy}^\sigma - (n_{xz}^\sigma + n_{yz}^\sigma)/2)$, is negative for the T_I structure ($p \sim -0.28$) and positive for the T_E structure ($p \sim 0.38$). The polarization sign flip does not depend on the specific choice of the energy window used to build the Wannier functions [19]. Rather, it arises from the relatively small differences in bandwidth/shape and crystal-field splitting between T_I and T_E structures. Switching on correlations only changes the orbital polarization a little. The small occupation transfer is associated with a corresponding small Coulomb-induced crystal-field modification. The latter is given by

$$
\Delta\varepsilon_{CF}(\omega) = \mathrm{Re}\,\Sigma_{xz/yz}^{\sigma\sigma}(\omega) - \mathrm{Re}\,\Sigma_{xy}^{\sigma\sigma}(\omega).
$$

The Hartree-Fock contribution to $\Delta\varepsilon_{CF}(\omega)$ is the infinite frequency limit $\Delta\varepsilon_{CF}(\infty) = (U - 5J)\frac{p}{2}$. The contribution relevant for the Fermi surface is, instead, the zero-frequency limit, $\Delta\varepsilon_{CF}(0)$. For Sr$_2RhO_4$, for all realistic Coulomb parameter choices, $|\Delta\varepsilon_{CF}(0)|$ is tiny—more specifically, 1–30 meV, depending on the values of U and J. Remarkably, we find that $\Delta\varepsilon_{CF}(0)$ can even become negative, i.e., can become a crystal-field *reduction*. Irrespective of its sign, $\Delta\varepsilon_{CF}(0)$ is much smaller than in the case of the t_{2g}^4 ruthenate Sr$_2$RuO$_4$, even for the T_E structure, which has an LDA crystal-field splitting similar in value to the one of Sr$_2$RuO$_4$. As a consequence, in the single-layered rhodate, $\Delta\varepsilon_{CF}(0)$ itself affects little the Fermi surface, while in the case of Sr$_2$RuO$_4$ is an essential ingredient [11].

Let us now analyze the open question of the interplay of SO interaction and correlations. If $\Delta_{CF}(0)$ is negligible, is then the LDA+U enhancement of the SO coupling indeed an artefact of the static mean-field approximation [8]? Our LDA+DMFT calculations show that this is not case. The effective SO-coupling enhancements are defined here as

$$
\frac{\Delta\lambda_z(\omega)}{2} = \mathrm{Im}\,\Sigma_{yz,xz}^{\uparrow\uparrow}(\omega),
$$
$$
\frac{\Delta\lambda_{xy}(\omega)}{2} = \mathrm{Re}\,\Sigma_{xy,yz}^{\uparrow\downarrow}(\omega).
$$

We find that $\Delta\lambda_{z/xy}(0) \sim 100 - 150$ meV, both for the idealized and the experimental tetragonal structure, i.e., the effective SO couplings are almost doubled with respect to the LDA values. The LDA+DMFT results for the Fermi surface are shown in Fig. 3, where the calculated Fermi surface is compared to available ARPES data. By comparing Figs. 3(a) and 3(c), one may see that correlations do little in the absence of SO interaction. This is because the self-energy only yields a negligible effective modification of the crystal-field splitting. Including the SO interaction improves the agreement with experiments already at the LDA level, as previously pointed out [7]. This may be seen comparing Figs. 3(a) and 3(b). The agreement becomes very good when Coulomb interaction effects are additionally taken into account [Fig. 3(d)]. We find that the actual values of $\Delta\lambda_{z/xy}(\omega)$ are influenced by the rotation of the octahedra, and the associated changes in occupations. Indeed, while for the T_I structure $\Delta\lambda_z(0) < \Delta\lambda_{xy}(0)$, for the T_E structure we find the opposite result, i.e., $\Delta\lambda_z(0) >$
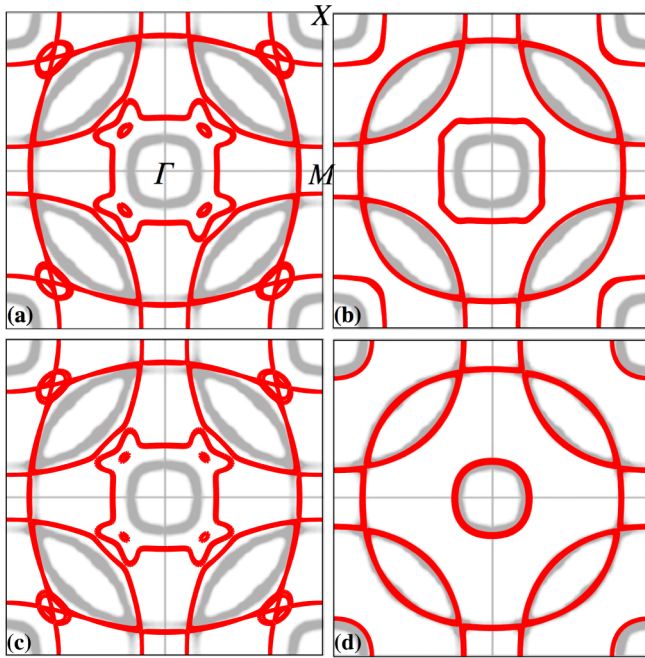
FIG. 3. The Fermi surface of Sr_2RhO_4 for the T_E (experimental) structure calculated with (a) LDA, (b) LDA+SO, (c) LDA+DMFT, and (d) LDA+SO+DMFT. Parameters $U = 2.3$ eV and $J = 0.4$ eV. The grey maps are experimental ARPES maps taken from Ref. [4].

FIG. 4. The Fermi surface of Sr_2RhO_4 calculated with LDA+SO+DMFT including the anisotropic Coulomb term ΔU. Parameters $U = 2.3$ eV, $J = 0.4$ eV, $\Delta U = -0.3$ eV. The grey maps are experimental ARPES maps taken from Ref. [4]. The Fermi surface is very close to the one shown in Fig. 3(d).

$\Delta\lambda_{xy}(0)$. A large part of the SO effective enhancement—although not all—can be ascribed to the static Hartree-Fock high-frequency self-energy terms; hence the enhanced SO anisotropy is associated in first approximation with the size of the off-diagonal occupation matrices. While in the T_I structure we obtain $|n_{xz,xy}| \sim 2|n_{xz,yz}|$, in the T_E case we find $|n_{xz,xy}| \sim |n_{xz,yz}|$, and a larger dynamical component. Thus, our results do confirm the SO enhancement found in static mean-field calculations. Still, the picture of the Fermi surface emerging from LDA+U results is only partially correct. Indeed, for given values of U and J, the Coulomb enhancement can be sizably overestimated within the approach adopted in Ref. [7]. This happens in part because of the specific form of the Coulomb tensor used (see discussion in Ref. [24] for the xz-yz density-density tensor and the Appendix for the complete t_{2g} tensor), and in part because dynamical effects are obviously neglected in static mean-field theory. Remarkably, once the effective enhancement of the SO interaction is taken into account, the Fermi surface in Fig. 3(d) is easy to understand. Indeed, leaving aside the band folding due to the supercell, in the very large SO coupling limit, the Fermi surface can be described, in first approximation, as the one arising from the two-dimensional bands:

$$E_{\pm}(\mathbf{k}) \sim \frac{\varepsilon_{xz}(\mathbf{k}) + \varepsilon_{yz}(\mathbf{k})}{2} \pm \frac{\lambda_z}{2}.$$

These yield two round Fermi surfaces, one electronlike and the other one holelike.

Once we have established these conclusions, we can now examine the effects of the nonspherical Coulomb terms. We extracted an estimate of ΔU from reported cRPA calculations in the total angular momentum basis [9], and then performed
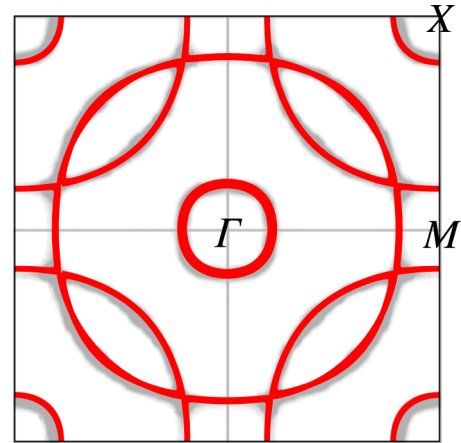
calculations in a very large interval around it (-0.45 eV $< \Delta U < 0.45$ eV). We find that, remarkably, contrary to the case of Sr_2RuO_4, the effect of ΔU on the crystal-field enhancement $\Delta\varepsilon_{CF}(0)$—and thus on the Fermi surface—is small for realistic values. This is because the xy orbital is almost fully occupied in the T_E structure, and it remains so unless ΔU becomes unrealistically large. The Fermi surface obtained with $\Delta U \sim -0.3$ eV, a value about two times larger than the cRPA estimate, is shown in Fig. 4.

B. Optical conductivity

The theoretical description of the optical conductivity experiments in Sr_2RhO_4 is currently controversial. It has been recently proposed that the midinfrared β peak at ~ 0.2 eV corresponds to an interband transition activated by the SO interaction [12]. A midinfrared peak similar to β has been observed also in the ruthenates,- although at somewhat lower energy. Thus, it has been argued that the SO-activated transition could be relevant for these systems as well [12]. This is in contrast to the strong-correlation picture emerging from early LDA+DMFT works, which neglects the effects of the SO interaction. In this picture, the β-like feature can be encompassed by the resilient quasiparticle scenario [13,25]. The new interpretation also differs from our recent LDA+SO+DMFT results, in which SO effects were accounted for. Indeed, for Sr_2RuO_4 we found that the effect of the SO interaction is particularly important at low—rather than midinfrared—frequency. Furthermore, we find that the intraorbital contributions remain large, although indeed the SO interaction does enhance the β-like peak via terms other than the intraorbital [14]. In the present paper, we therefore examine in detail the case of Sr_2RhO_4 and compare it to Sr_2RuO_4. Our LDA+DMFT results for the in-plane $\sigma_{ab}(\omega)$ and out-of-plane $\sigma_c(\omega)$ conductivity are shown in Fig. 5 together with available experimental data. First of all, the agreement between theory and experiments is overall good, in particular we do indeed find a peak at about 0.2 eV, the location of the β feature, in
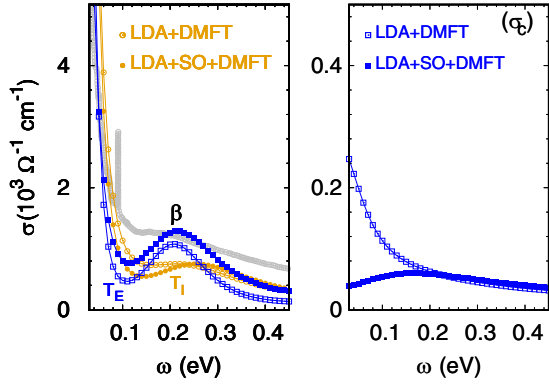
FIG. 5. The in-plane [$\sigma_{ab}(\omega)$] and out-of-plane [$\sigma_c(\omega)$] optical conductivity of Sr_2RhO_4 for the T_E (square) and T_I (circles) structure. Empty symbols: LDA+DMFT. Filled symbols: LDA+SO+DMFT. Parameters $U = 2.3$ eV, $J = 0.4$ eV, $\Delta U = 0$. The grey points are experimental data from Ref. [12]. The calculations are performed at ~200 K, the temperature of the experimental data.

line with the data [12]. This peak is present both with and without SO interaction, and both for the T_I and T_E structures, although it moves to lower energy and becomes stronger for the T_E structure with SO interaction. The sharp feature in the experiments at around ~80 meV has been identified with an optical phonon [12] and, indeed, in line with this interpretation, it is not reproduced in the theoretical electronic conductivity calculated in this paper.

Let us now examine in more detail the influence of the SO interaction on the optical response. For the T_E structure, the static value $\sigma_{ab}(0)$ is reduced and β feature is enhanced by the SO coupling. Instead, in the absence of rotations of the octahedra, for the idealized T_I structure, at low frequency the conductivity is slightly enhanced by the SO interaction, while the β peak is somewhat suppressed. This may be seen in the left panel of Fig. 5. The origin of this apparently opposite behavior can be understood after splitting the contributions to the transport function in three different channels [14]. These channels are T_{intra}, the sum of all the intraorbital terms, T_{inter}, the interorbital term, defined as

$$T_{inter} = \frac{2\pi}{V} \sum_{\mathbf{k}, m \neq m'} \left[\mathbf{v}_{m',m}^{\mathbf{k}} A_{m,m}^{\mathbf{k}}(\omega + \omega') \mathbf{v}_{m,m'}^{\mathbf{k}} A_{m',m'}^{\mathbf{k}}(\omega) \right],$$

and T_{rest}, which contains all the terms that cannot be classified as pure intra- or interorbital. The result of the splitting is shown in Fig. 6.

In the presence of the SO interaction, a large weight shifts from T_{intra} to the T_{inter} and the T_{rest} channels, as can be seen clearly at low frequency. Such a weight transfer happens also in Sr_2RuO_4, as we have shown in Ref. [14]; however, in this material the effect is weaker. For Sr_2RhO_4, already in the T_I structure the contribution of the T_{rest} channel is larger than in Sr_2RuO_4. At the same time, the intraorbital processes are reduced to about half their values. This is what one expects even in the uncorrelated case, as a consequence of a moderate SO-induced orbital mixing. Despite the reduction, the intraorbital terms remain important with respect to other processes, and contribute in a relevant way
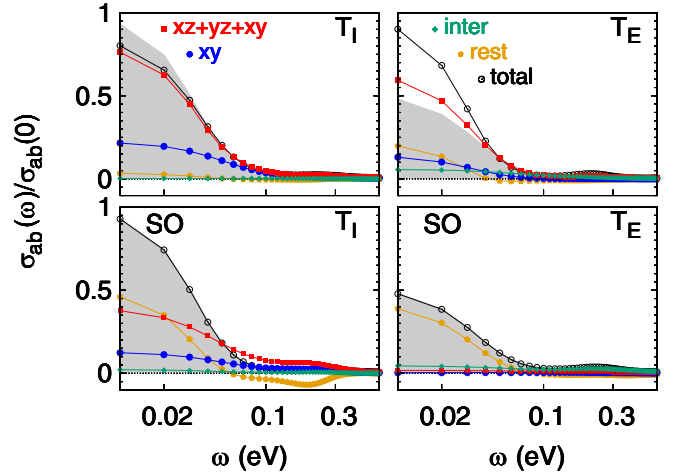

FIG. 6. In-plane optical conductivity of Sr_2RhO_4 for the T_I (left) and T_E (right) structures split into components. Coulomb parameters and temperature are the same as in Fig. 5. All curves are normalized to $\sigma_{ab}(0)$ for the T_I structure with spin-orbit interaction. Circles: Intraorbital xy term. Squares: Total intraorbital term. Diamonds: Interorbital term. Empty circles: Total. Pentagons: Remaining contributions. Top panels: LDA+DMFT. Bottom panels: LDA+SO+DMFT. Filled grey curve: Total with spin-orbit interaction.

at energies around the β peak. The β feature is suppressed by the SO interaction because, although both intraorbital and interorbital contributions increase at β with respect to the case without SO interaction, the increase is overcompensated by the large T_{rest}. This can be seen in the left panels of Fig. 6. The shift of weight further increases for the experimental T_E structure, however. Here the T_{rest} term determines the $\sigma_{ab}(0)$ value, since the remaining terms are small. T_{rest} is also the term that controls the overall shape of the conductivity. If we now focus on the β peak, the two terms that contribute are T_{inter} and T_{rest}, and T_{inter} dominates. Hence, the SO interaction enhances the β feature. This can be seen in the right panels of Fig. 6. Summarizing, Fig. 6 shows that the effect of the SO interaction is in reality similar for Sr_2RuO_4 and Sr_2RhO_4, or for the T_I and T_E structures, the difference being quantitative rather than qualitative; in the case of the T_I structure, the SO-induced weight shift to T_{rest} and T_{inter} is partial, while it is very large in the T_E case. However, the large weight transfer also indicates that, as suggested in Ref. [12], the t_{2g} single-orbital picture is not applicable to describe conductivity data in Sr_2RhO_4, even though it can be still used for Sr_2RuO_4. In the large SO coupling limit, switching from the t_{2g} basis to the basis of the atomic $\Gamma_7 - \Gamma_6$ spinor states (see Refs. [24,26] for the expressions), one can see that the term T_{rest} contributes to both intra and interspinor terms. For the β peak itself, we underline that a β-like peak is present also in the absence of SO coupling. Indeed, the rotations of the octahedra shown in Fig. 1 already yield alone a sizable β feature. Our results show that the SO interaction enhances rather than generates the peak, while at the same time it has a drastic effect on the distribution of weights at low energy. This can be seen in Figs. 5 and 6. The figure also shows that the out-of-plane conductivity $\sigma_c(\omega)$ is strongly suppressed by the SO
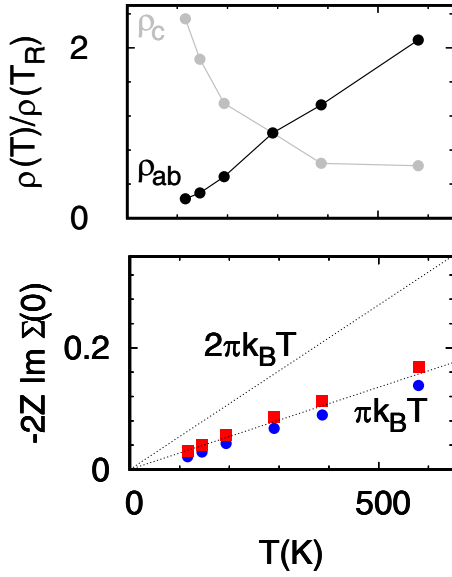
FIG. 7. Temperature dependence of the resistivity (normalized to the room temperature value) and scattering rates. The resistivity is obtained from the zero-frequency conductivity in Fig. 5. The scattering rate is extracted from the imaginary frequency self-energy. For the latter, circles are xy and squares xz/yz terms. All calculations are done with spin-orbit interaction and for the T_E structure. The coulomb parameters are the same of Fig. 5.

interaction at low frequencies; this happens both for the T_E and the idealized T_I structure.

To complete the discussion, we analyze the effects of temperature on quantities relevant for either the Fermi surface or transport. Figure 7 shows that the scattering rate scales as $\sim \pi k_B T$ in the full considered temperature range, i.e., it is linear in T as in the case of the single-layered ruthenates, but its value is much closer to the weakly correlated limit. This is reflected in the temperature dependence of the in-plane resistivity. The scattering rate is larger for the xz/yz orbitals, in accord with the larger effective masses and the fact that the xy orbital is almost full. The remaining relevant parameters can be found in Fig. 8. The figure shows that the masses slightly decrease with temperature, while correspondingly the xy occupation increases. This is in line with the fact that the system progressively approaches the xy^2 configuration. The SO enhancements $\Delta\lambda_\alpha(0)$, down to 100 K, do not depend strongly on the temperature.

Figure 9 shows the dependence of the parameters on ΔU. The effective mass enhancement m^*_{xy}/m_{xy} is weakly influenced by a large negative $\Delta U = -0.45$ eV, which merely increases slightly the occupation n_{xy}; further increasing $|\Delta U|$, eventually, the xy band becomes fully occupied and thus insulating. Instead, a large positive $\Delta U \sim 0.45$ eV, which enhances the weight of xy^1 configurations, can enhance m^*_{xy}/m_{xy} up to the value 4.0. For the xz masses, the opposite happens. In an extreme case, with an unrealistic $\Delta U \sim -0.45$ eV, we find $m^*_{xz/yz} \sim 4.5$. At the same time, idealized DMFT calculations performed using the Hamiltonian of Sr_2RuO_4, setting $\Delta U = 0$ and the electronic t_{2g}^5 configuration, do yield masses as small as obtained in Sr_2RhO_4. For what concerns the static conductivity and the average SO enhancement, Fig. 9 shows
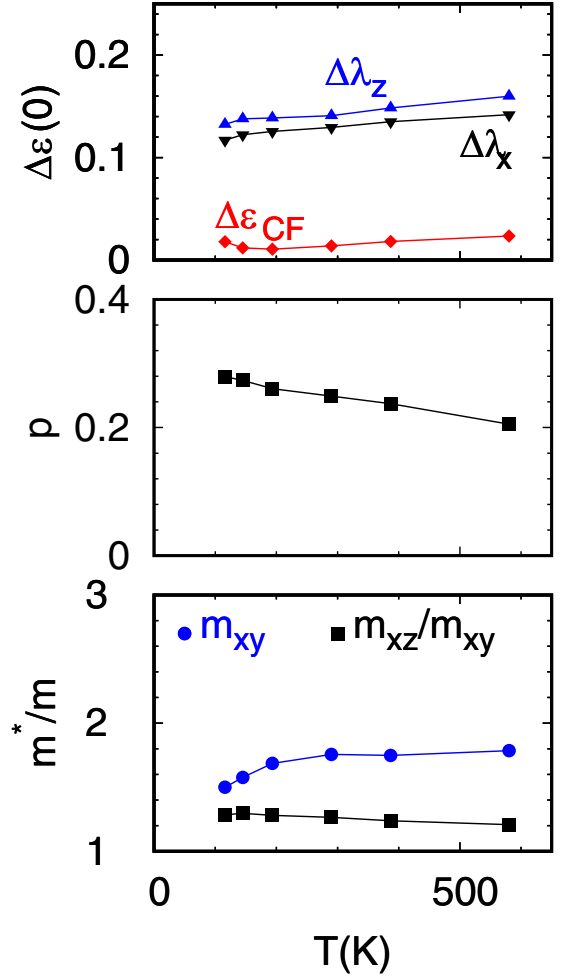

FIG. 8. Temperature dependence of various quantities, T_E structure. Top: Zero-energy self-energy parameters relevant for the Fermi surface. Middle: Orbital polarization. Bottom: Effective mass enhancement m^*_{xy}/m_{xy} and ratio $m^*_{xz/yz}/m^*_{xy}$. The combined effect of the large $\Delta\lambda_{xy}(\omega)$ and small $\Delta\varepsilon_{CF}(\omega)$ yields a slight decrease in orbital polarization with respect the LDA+SO values. On lowering the temperature, the xy orbital slowly increases toward full occupation ($n_{xy} = 2$, $p = 0.5$). Calculations are all for the experimental T_E structure and include spin-orbit coupling.

that, varying ΔU, $\sigma_{ab}(0)$ decreases when $\Delta\lambda(0)$ increases, in line with the observations already made for Fig. 6. It has to be noticed once more, however, that in Fig. 9 the tetragonal term ΔU varies in a very large window, $|\Delta U| < 0.45$ eV; as previously pointed out, cRPA yields rather $|\Delta U| \sim 0.1$ eV or smaller. For such values, the effect of ΔU is small on all quantities. Finally, we find that, in the analyzed temperature range, the effective masses change little with and without SO coupling for all realistic values of the Coulomb parameters.

IV. CONCLUSION

In this paper, we reexamined the electronic structure of Sr_2RhO_4 via the LDA+DMFT method. We used a general interaction-expansion CT-QMC DMFT solver which allows us to perform exact calculations, including both the SO interaction and tetragonal Coulomb terms. We find
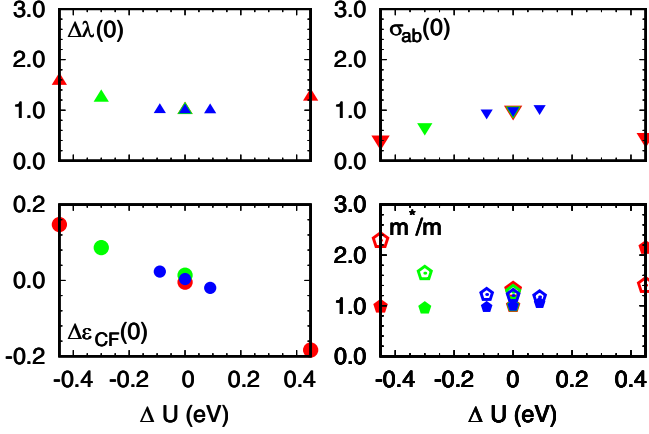
FIG. 9. Effect of ΔU on representative quantities (290 K, T_E structure). Symbols of increasing size correspond to increasing (U, J): $(1.8, 0.3)\,\mathrm{eV} \longrightarrow (2.3, 0.4)\,\mathrm{eV} \longrightarrow (3.1, 0.7)\,\mathrm{eV}$. Top: Average spin-orbit enhancement (left) and zero-frequency conductivity (right), renormalized to their $\Delta U = 0$ values. Bottom, left: Crystal-field "enhancement" in eV. Bottom, right: Effective mass enhancements, renormalized to m^*_{xy}/m_{xy} for $\Delta U = 0$; empty symbols: $m^*_{xz/yz}/m_{xz/yz}$; full symbols m^*_{xy}/m_{xy}.

that the Coulomb interaction only yields a tiny enhancement/reduction of the crystal field at zero frequency, differently than in the case of Sr_2RuO_4. We find that instead the electron-electron repulsion does lead to an effective doubling of the SO couplings at zero frequency. This supports the picture emerging from early LDA+U results [7], even if we find that in LDA+U calculations the effect is overestimated [24]. We also find that the tetragonal Coulomb term ΔU, for realistic values, does not affect sizably neither the Fermi surface nor other Fermi-liquid properties. In the second part of this paper, based on this, we have then studied the electronic contribution to the optical conductivity. The interpretation of optical conductivity experiments has been recently a subject of debate [12]. Our results reproduce well not only the Drude peak, but also the β feature found in recent experiments. We show that the conductivity is dominated by terms which involve t_{2g} off-diagonal elements of the spectral function matrix and/or of the velocity matrix. Instead, the intraorbital processes play a small role. This changes the way in which the conductivity data should be interpreted, since it is not possible to discuss the experimental results in terms of separate single t_{2g} orbital contributions. This agrees with the recent proposal made in Ref. [12]. We find, however, that in this respect, the case of Sr_2RhO_4 is different from that of Sr_2RuO_4; in the latter, the intraorbital terms remain large, even in the presence of the SO interaction [14]. We show furthermore that the β feature is already present in the absence of the SO interaction, which enhances, rather than generates, the peak.

ACKNOWLEDGMENTS

APPENDIX

In this Appendix, we give explicitly the complete form of the spherical Coulomb tensor for t_{2g} electrons in the total angular momentum basis. In spherical symmetry, the Coulomb interaction tensor for t_{2g} states is given by

$$
\hat{H}_U = U \sum_m n_{m\uparrow} n_{m\downarrow}
$$

$$
+ U' \sum_{m \neq m'} n_{m\uparrow} n_{m'\downarrow} + (U' - J) \sum_{m\sigma < m'\sigma} n_{m\sigma} n_{m'\sigma}
$$

$$
+ J \sum_{m \neq m'} c^\dagger_{m\uparrow} c^\dagger_{m'\downarrow} c_{m\downarrow} c_{m'\uparrow} + J \sum_{m \neq m'} c^\dagger_{m\uparrow} c^\dagger_{m\downarrow} c_{m'\downarrow} c_{m'\uparrow},
$$

where $U' = U - 2J$. The t_{2g} creation operators can be expressed as follows in the total angular momentum basis:

$$
c^\dagger_{xy;\uparrow} = \frac{i}{\sqrt{3}} \left[+\sqrt{2} c^\dagger_{\frac{1}{2}} - d^\dagger_{\frac{1}{2}} \right],
$$

$$
c^\dagger_{xy;\downarrow} = \frac{i}{\sqrt{3}} \left[+\sqrt{2} c^\dagger_{-\frac{1}{2}} + d^\dagger_{-\frac{1}{2}} \right],
$$

$$
c^\dagger_{yz;\uparrow} = \frac{i}{\sqrt{6}} \left[-\sqrt{3} c^\dagger_{\frac{3}{2}} + c^\dagger_{-\frac{1}{2}} - \sqrt{2} d^\dagger_{-\frac{1}{2}} \right],
$$

$$
c^\dagger_{yz;\downarrow} = \frac{i}{\sqrt{6}} \left[+\sqrt{3} c^\dagger_{-\frac{3}{2}} - c^\dagger_{\frac{1}{2}} - \sqrt{2} d^\dagger_{\frac{1}{2}} \right],
$$

$$
c^\dagger_{xz;\uparrow} = \frac{1}{\sqrt{6}} \left[-\sqrt{3} c^\dagger_{\frac{3}{2}} - c^\dagger_{-\frac{1}{2}} + \sqrt{2} d^\dagger_{-\frac{1}{2}} \right],
$$

$$
c^\dagger_{xz;\downarrow} = \frac{1}{\sqrt{6}} \left[-\sqrt{3} c^\dagger_{-\frac{3}{2}} - c^\dagger_{\frac{1}{2}} - \sqrt{2} d^\dagger_{\frac{1}{2}} \right].
$$

Here the $d^\dagger_{m_j}$ ($c^\dagger_{m_j}$) operators create electrons with $j = 1/2$ ($j = 3/2$). The latter are defined in terms of creators of the effective p states,

$$
p^\dagger_{+1;\sigma} = -\frac{c^\dagger_{xz;\sigma} - i c^\dagger_{yz;\sigma}}{\sqrt{2}},
$$

$$
p^\dagger_{0;\sigma} = -i c^\dagger_{xy;\sigma},
$$

$$
p^\dagger_{-1;\sigma} = -\frac{c^\dagger_{xz;\sigma} + i c^\dagger_{yz;\sigma}}{\sqrt{2}},
$$

so

$$
c^\dagger_{\pm\frac{3}{2}} = p^\dagger_{\pm 1;\pm\frac{1}{2}},
$$

$$
c^\dagger_{\pm\frac{1}{2}} = \frac{p^\dagger_{\pm 1;\mp\frac{1}{2}} + \sqrt{2} p^\dagger_{0;\pm\frac{1}{2}}}{\sqrt{3}},
$$

$$
d^\dagger_{\pm\frac{1}{2}} = \pm \frac{\sqrt{2} p^\dagger_{\pm 1;\mp\frac{1}{2}} - p^\dagger_{0;\pm\frac{1}{2}}}{\sqrt{3}}.
$$

In the new basis, the Coulomb Hamiltonian is made of two terms, $\hat{H}_U = \hat{H}^U + \hat{H}^J$. The first is proportional to U and it is

given by

$$\hat{H}^U = U \sum_j \sum_{m_j < m'_j} n^j_{m_j} n^j_{m'_j} + U \sum_{m_{\frac{1}{2}}, m_{\frac{3}{2}}} n^{\frac{1}{2}}_{m_{\frac{1}{2}}} n^{\frac{3}{2}}_{m_{\frac{3}{2}}},$$

where $m_j = -j, \dots, +j$. The second term, proportional to J, can be split into a density-density operator

$$\hat{H}^J_1 = -J \sum_{j_1 m_{j_1} > j_2 m_{j_2}} \alpha_{j_1 m_{j_1}, j_2 m_{j_2}} n^{j_1}_{m_{j_1}} n^{j_2}_{m_{j_2}},$$

where, ordering the states in decreasing order of j, m_j,

$$\alpha_{j_1 m_{j_1}, j_2 m_{j_2}} = \frac{1}{3} \begin{pmatrix} 0 & 7 & 7 & 3 & 5 & 8 \\ 7 & 0 & 3 & 7 & 6 & 7 \\ 7 & 3 & 0 & 7 & 7 & 6 \\ 3 & 7 & 7 & 0 & 8 & 5 \\ 5 & 6 & 7 & 8 & 0 & 4 \\ 8 & 7 & 6 & 5 & 4 & 0 \end{pmatrix}.$$

In addition, there is a weighted hopping operator,

$$\hat{H}^J_2 = -J \sum_{p=-\frac{3}{2}}^{\frac{3}{2}} \sum_{\sigma=-\frac{1}{2}}^{\frac{1}{2}} \beta_{p,\sigma} n^{\frac{3}{2}}_{(-1)^{\delta_{p\sigma}} p} (c^\dagger_\sigma d_\sigma + d^\dagger_\sigma c_\sigma),$$

where $\beta_{p,\sigma} = -\frac{\sqrt{2}}{3}(-1)^{\delta_{p\sigma}}(p+\sigma)$. The remaining Coulomb terms can be written as

$$\begin{aligned}
\hat{H}^J_3 = -\frac{J}{3}\Bigg\{ & 5c^\dagger_{\frac{1}{2}} c^\dagger_{-\frac{1}{2}} d_{-\frac{1}{2}} d_{\frac{1}{2}} + 5c^\dagger_{\frac{3}{2}} c^\dagger_{-\frac{3}{2}} d_{\frac{1}{2}} d_{-\frac{1}{2}} \\
& + 4 c^\dagger_{\frac{3}{2}} c^\dagger_{-\frac{3}{2}} c_{-\frac{1}{2}} c_{\frac{1}{2}} + 2 c^\dagger_{-\frac{1}{2}} d^\dagger_{\frac{1}{2}} c_{\frac{1}{2}} d_{-\frac{1}{2}} \\
& + \sqrt{2} c^\dagger_{\frac{3}{2}} c^\dagger_{-\frac{3}{2}} (c_{-\frac{1}{2}} d_{\frac{1}{2}} + c_{\frac{1}{2}} d_{-\frac{1}{2}}) \\
& + \sqrt{3} \sum_{\sigma=-\frac{1}{2}}^{\frac{1}{2}} 2\sigma c^\dagger_\sigma d^\dagger_\sigma c_{3\sigma} (\sqrt{2} c_{-\sigma} + 2\sigma d_{-\sigma}) \Bigg\} + \text{H.c.}
\end{aligned}$$

In the literature, terms without the density-density form are often neglected. Furthermore, in some cases, approximated forms of the density-density couplings are used. This might, in specific cases, lead to overestimates of Coulomb Hartree-Fock terms. See Ref. [24] for a discussion of an example. We point out that the form of the Coulomb tensor changes in the $\Gamma_7 - \Gamma_6$ basis obtained with finite crystal field (see Refs. [14,26] for the analytic expression), since its components are not invariant under unitary transformations.

[1] T. Vogt and D. J. Buttrey, J. Solid State Chem. **123**, 186 (1996).

[2] R. S. Perry, F. Baumberger, L. Balicas, N. Kikugawa, N. J. C. Ingle, A. Rost, J. F. Mercure, Y. Maeno, Z. X. Shen, and A. P. Mackenzie, New J. Phys. **8**, 175 (2006).

[3] F. Baumberger, N. J. C. Ingle, W. Meevasana, K. M. Shen, D. H. Lu, R. S. Perry, A. P. Mackenzie, Z. Hussain, D. J. Singh, and Z.-X. Shen, Phys. Rev. Lett. **96**, 246402 (2006).

[4] B. J. Kim, J. Yu, H. Koh, I. Nagai, S. I. Ikeda, S.-J. Oh, and C. Kim, Phys. Rev. Lett. **97**, 106401 (2006).

[5] E. Ko, B. J. Kim, C. Kim, and H. J. Choi, Phys. Rev. Lett. **98**, 226401 (2007).

[6] M. W. Haverkort, I. S. Elfimov, L. H. Tjeng, G. A. Sawatzky, and A. Damascelli, Phys. Rev. Lett. **101**, 026406 (2008).

[7] G.-Q. Liu, V. N. Antonov, O. Jepsen, and O. K. Andersen, Phys. Rev. Lett. **101**, 026408 (2008).

[8] K.-A. Ahn, K.-W. Lee, and J. Kunes, J. Phys.: Condens. Matter. **27**, 085602 (2015).

[9] L. Vaugier, H. Jiang, and S. Biermann, Phys. Rev. B **86**, 165105 (2012); notice that the U tensor for Sr$_2$RhO$_4$ given in this paper for the T_I structure apparently does not fulfill tetragonal symmetry.

[10] C. Martins, M. Aichhorn, and S. Biermann, J. Phys.: Condens. Matter **29**, 263001 (2017); the calculations for the T_E structure are performed in the $\Gamma_7 - \Gamma_6$ basis which diagonalizes the initial local Green's function, which is kept frozen in the self-consistency (off-diagonal elements are neglected). This basis is called effective j-basis in the paper. The analytic expression of the basis for a general crystal-field splitting can be found in Refs. [14,26]. Notice that the Coulomb density-density interaction explicitly given in Eq. (20) of the paper is in the basis of the total angular momentum. The cRPA values given in the paper are for the T_I structure.

[11] G. Zhang, E. Gorelov, E. Sarvestani, and E. Pavarini, Phys. Rev. Lett. **116**, 106402 (2016).

[12] L. J. Sandilands, W. Kyung, S. Y. Kim, J. Son, J. Kwon, T. D. Kang, Y. Yoshida, S. J. Moon, C. Kim, and T. W. Noh, Phys. Rev. Lett. **119**, 267402 (2017).

[13] D. Stricker, J. Mravlje, C. Berthod, R. Fittipaldi, A. Vecchione, A. Georges, and D. van der Marel, Phys. Rev. Lett. **113**, 087404 (2014).

[14] E. Sarvestani, G. Zhang, E. Gorelov, and E. Pavarini, Phys. Rev. B **97**, 085141 (2018).

[15] For a pedagogical introduction see, e.g., *The LDA+DMFT Approach to Strongly Correlated Materials*, Reihe Modeling and Simulation Vol. 1, edited by E. Pavarini, E. Koch, D. Vollhardt, and A. Lichtenstein (Verlag des Forschungszentrum Jülich, Jülich, Germany, 2011). For the Coulomb tensor for t_{2g} states, see Chapter 6: https://www.cond-mat.de/events/correl11/manuscripts/pavarini.pdf.

[16] P. Blaha, K. Schwarz, G. K. H. Madsen, D. Kvasnicka, and J. Luitz, *WIEN2K, An Augmented Plane Wave + Local Orbitals Program for Calculating Crystal Properties* (Technische Universität Wien, Austria, 2001); P. Blaha, K. Schwarz, P. Sorantin, and S. Trickey, Comput. Phys. Commun. **59**, 399 (1990).

[17] N. Marzari and D. Vanderbilt, Phys. Rev. B **56**, 12847 (1997).

[18] For the Wannier90 code, see A. A. Mostofi, J. R. Yates, Y.-S. Lee, I. Souza, D. Vanderbilt, and N. Marzari, Comput. Phys. Commun. **178**, 685 (2008); for the interface to WIEN2K, see J. Kuneš, R. Aryta, P. Wissgott, A. Toschi, H. Ikeda, and K. Held, **181**, 1888 (2010).

[19] More specifically, the value depends on the choice of the low-energy bands included in building the Wannier functions. Results in different bases do not change too much, but differences

are comparable with those obtained with different choices of (U, J) in the range from $(1.8, 0.2)$ eV to $(3.1, 0.7)$ eV.

[20] E. Gull, A. J. Millis, A. I. Lichtenstein, A. N. Rubtsov, M. Troyer, and P. Werner, Rev. Mod. Phys. **83**, 349 (2011).

[21] A. N. Rubtsov, V. V. Savkin, and A. I. Lichtenstein, Phys. Rev. B **72**, 035122 (2005).

[22] A. Flesch, E. Gorelov, E. Koch, and E. Pavarini, Phys. Rev. B **87**, 195141 (2013).

[23] E. Gorelov, M. Karolak, T. O. Wehling, F. Lechermann, A. I. Lichtenstein, and E. Pavarini, Phys. Rev. Lett. **104**, 226401 (2010).

[24] G. Zhang and E. Pavarini, Phys. Rev. B **95**, 075145 (2017).

[25] X. Deng, K. Haule, and G. Kotliar, Phys. Rev. Lett. **116**, 256401 (2016).

[26] G. Zhang and E. Pavarini, Phys. Status Solidi RRL **12**, 1800211 (2018).